Orbital-selective confinement effect of Ru 4*d* orbitals in $SrRuO_3$ ultrathin film

Soonmin Kang,[1,2] Yi Tseng,[3] Beom Hyun Kim,[4] Seokhwan Yun,[1,2] Byungmin Sohn,[1,2] Bongju Kim,[1,2] Daniel McNally,[3] Eugenio Paris,[3] Choong H. Kim,[1,2] Changyoung Kim,[1,2] Tae Won Noh,[1,2] Sumio Ishihara,[5] Thorsten Schmitt,[3,*] and Je-Geun Park[1,2,†]

[1]*Center for Correlated Electron Systems, Institute for Basic Science, Seoul 08826, Korea*
[2]*Department of Physics and Astronomy, Seoul National University, Seoul 08826, Korea*
[3]*Swiss Light Source, Paul Scherrer Institut, CH-5232 Villigen, Switzerland*
[4]*Korea Institute for Advanced Study, Seoul 02455, Korea*
[5]*Department of Physics, Tohoku University, Sendai 980-8578, Japan*

(Received 2 August 2018; published 7 January 2019)

The electronic structure of $SrRuO_3$ thin film with a thickness from 1 to 50 unit cell (u.c.) is investigated via the resonant inelastic x-ray scattering (RIXS) technique at the O *K* edge to unravel the intriguing interplay of orbital and charge degrees of freedom. We found that the orbital-selective quantum confinement effect (QCE) induces the splitting of Ru 4*d* orbitals. At the same time, we observed a clear suppression of the electron-hole continuum across the metal-to-insulator transition occurring in the 4-u.c. sample. From these two clear observations we conclude that the QCE gives rise to a Mott insulating phase in ultrathin $SrRuO_3$ films. Our interpretation of the RIXS spectra is supported by the configuration interaction calculations of RuO_6 clusters.

DOI: 10.1103/PhysRevB.99.045113

I. INTRODUCTION

The orbital degree of freedom (DOF) is relatively less well understood among the four fundamental DOFs of solids: charge, spin, lattice, and orbital. The role of the orbital DOF was originally recognized by the now famous Kugel-Khomskii model [1]. It took another decade before its full consequence was experimentally observed from numerous studies on so-called colossal magnetoresistance (CMR) manganites [2]. The most direct effect of the orbital DOF can be found in the so-called orbital ordering and the associated metal-insulator transition (MIT) with unique magnetic or structural transitions [3,4]. A more recent breakthrough in the understanding of the orbital DOF is in the discovery of the orbital-selective mechanism. It is now believed that several Ru and V oxides exhibit the phenomena that arise from the orbital-selective physics [4–7]. One notable example is the orbital-selective Mott transition [8].

The role of the orbital DOF is typically enhanced for localized systems, i.e., with a larger *U* term. So it becomes more prominent in 3*d* transition-metal oxides, which is why CMR manganite was the first system that was identified with orbital physics. Nevertheless, several Ru compounds were also reported to have rather unique features due to the orbital physics. Despite the progress in our understanding of the orbital physics of Ru, an orbital-selective process still remains pretty much unexplored for Ru compounds, although it was already suggested for the doping-dependent MIT of $(Ca,Sr)_2RuO_4$ [5,9,10].

$SrRuO_3$ is a well-known member of the ruthenate family with a ferromagnetic phase below a Curie temperature of 165 K. Unlike other ferromagnetic materials, the conductivity of bulk $SrRuO_3$ is high enough to make it a popular choice of electrode for various thin-film samples with a stable perovskite structure [11]. At the same time, it is one of the rare itinerant ferromagnetic oxides and has attracted significant interest in its own right [12,13]. For example, it has long been suspected that some kind of coupling between the lattice and spin degrees of freedom works for the ferromagnetic ground state. It was also found both theoretically and experimentally that RuO_6 octahedra of $SrRuO_3$ undergo quite irregular plastic distortion below the ferromagnetic transition temperature [14,15]. More recently, the unusual temperature dependence of the spin gap found by inelastic neutron scattering was attributed to a possible magnetic monopole in the *k* space [16]. Interestingly, it is known too that the metallic phase of bulk $SrRuO_3$ is close to a transition between Fermi-liquid and non-Fermi-liquid states [12,17]. Another interesting point, more relevant to our work, is that $SrRuO_3$ thin films undergo MIT with decreasing thickness, whose origin is, to date, not well understood [18–20]. Thus, $SrRuO_3$ thin films can be a fertile ground for exploring some of the fundamental physics related to MIT and correlation physics with the orbital DOF.

In addition, first-principles local-density approximation + *U* calculations found that the Ru orbitals of $SrRuO_3$ thin films exhibit rather unusual quantum confinement effects (QCEs) when reducing thickness [20]. As the thickness of the film gets reduced, the proportion of RuO_6 octahedra exposed to the surface increases, which makes Ru t_{2g} orbitals like d_{xz} or d_{yz} prefer to form one-dimensional (1D) strips. As a result of the geometrical restriction, the enhanced QCE was theoretically predicted to induce a distinctive change in the electronic structures for Ru 4*d* orbitals. To be more specific, the density

*thorsten.schmitt@psi.ch
†jgpark10@snu.ac.kr

of states (DOS) for a two-dimensional (2D) square lattice with a tight-binding model has a Van Hove singularity at the band center, whereas the DOS for a 1D line case has two separate singularities one at each edge of the band [21]. For example, the 2D-type Van Hove singularity of d_{xy} DOS persists down to monolayer $SrRuO_3$. However, d_{xz} and d_{yz} orbitals in the monolayer limit do not have electron hopping along the z axis due to spatial confinement, which induces the 1D-type singularities of their DOS. This orbital-selective QCE was theoretically suggested to be the main driving force of the intriguing paramagnetic phase found for very thin $SrRuO_3$ samples [20]. We also note that the QCE was used to explain the Mott insulating phase of $LaNiO_3/LaAlO_3$ thin films [22].

The purpose of this study was twofold. First, we investigated the proposed QCE by measuring the orbital-dependent charge transfer with the high-resolution resonant inelastic x-ray scattering (RIXS) studies as a function of thickness. Second, we studied how the charge dynamics changes across the MIT by examining low-energy excitations across the critical thickness. Furthermore, we tried to find a correlation between those two distinct characteristics of the $SrRuO_3$ thin film.

II. EXPERIMENTAL METHODS

Epitaxial $SrRuO_3$ thin films were deposited on TiO_2-terminated $SrTiO_3$ (001) substrates by pulsed-laser deposition at 670 °C with an oxygen pressure of 100 mTorr. Ultraviolet light coming from the excimer laser with a power of 2.1 J/cm^2 is applied to the target with a spot size of 2 mm^2. We optimized the growth conditions by measuring the resistivity of our samples and thereby monitoring the quality in addition to the usual inspection of the reflection high-energy electron diffraction (RHEED) patterns. The RHEED pattern in time variation implies good surface quality, which shows a clear change in the growth mode from a layer-by-layer growth to a step flow growth as a function of time. On the other hand, the high residual resistivity ratio of 8.2 obtained for the samples attests to the high-quality of our samples. In addition to the resistivity measurement, we verified the roughness of the samples in atomic force microscopy (AFM) images, another sign of the high quality of the surface in thin films (Fig. 1).

We carried out O K-edge RIXS at the ADRESS beamline of the Swiss Light Source [23,24]. RIXS is a powerful tool to study the charge dynamics related to orbital physics as one can tune the energy to a specific absorption resonance of the elements. The energy of the ruthenium L edge (∼3 keV), however, just happens to be situated in between soft and hard x-ray regimes. For this technical reason, it is not easy to get enough photon flux and energy resolution at the Ru L edge, which makes it experimentally challenging to do RIXS at the Ru L edge. Instead, we carried out our experiment at the oxygen K edge to study the charge dynamics of the Ru 4d orbitals while varying the thickness of thin-film samples.

The proper energy of the incident beam was chosen through x-ray absorption spectroscopy (XAS) with different thicknesses from 1 to 33 unit cells (u.c.), as shown in Fig. 2. The first peak at around 529.8 eV gets weaker as the thickness of the samples becomes reduced. From the fact that the relative intensity changes for different samples and

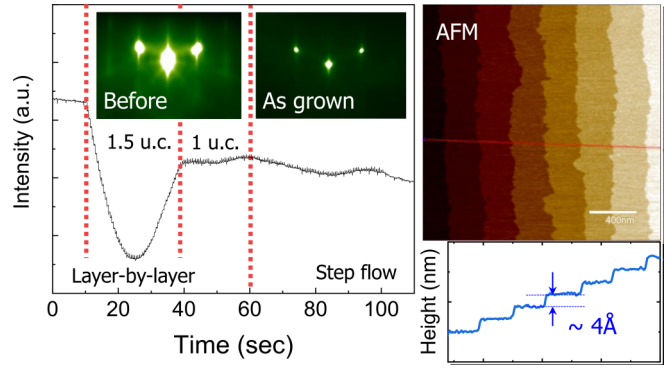

FIG. 1. *In situ* RHEED pattern and topography image with AFM. The sample growth starts from 10 s. The growth mode change that occurs at 40 and 60 s shows the good surface quality of thin films. The insets show RHEED patterns before and after the sample growth. The AFM image indicates the clean surface and the apparent steps with a height of 4 Å, which is the size of 1 u.c. for $SrRuO_3$.

also based on previous XAS studies in $SrTiO_3$ [25,26], we conclude that peaks above 530 eV are due to absorptions from the substrates. Therefore, we chose 529.8 eV as the incident energy for our RIXS experiment with high statistics, which is slightly lower than the pure O K edge. The energy difference between the pure O K edge and absorption from our sample comes from the hybridization energy. We verified the energy resolution is less than 70 meV by checking the full width at half maximum of the elastic line from diffuse scattering at a carbon tape reference.

All our samples were aligned with a grazing angle ($\theta = 15°$) to increase the scattering cross section especially for ultrathin samples. The scattering angle from the incident beam to the detector was fixed to 130°, with a corresponding momentum transfer of $\mathbf{q}_\parallel = 0.28[2\pi/a]$. We employed two different polarizations for our experiments: σ polarization is parallel to the sample plane, and π polarization is nearly perpendicular to the plane. Thus, the former is more sensitive to the p_x (p_y) orbital, while the latter is more sensitive to the p_z orbital due to the incident angle. All experiments were performed at 20 K.

Figure 3 shows RIXS results for all seven samples with different thicknesses. To explain the RIXS spectra, we divided the spectra into two groups depending on the characteristic

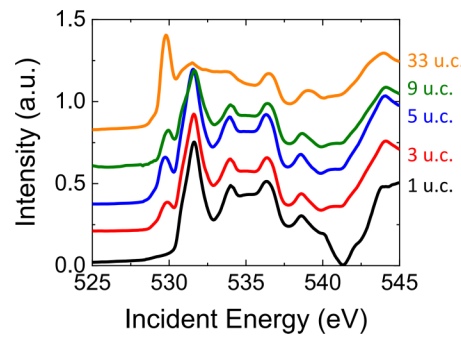

FIG. 2. XAS results as a function of the thickness of the sample. An energy of 529.8 eV was used for our RIXS experiments because other peaks mainly originate from the $SrTiO_3$ substrate.

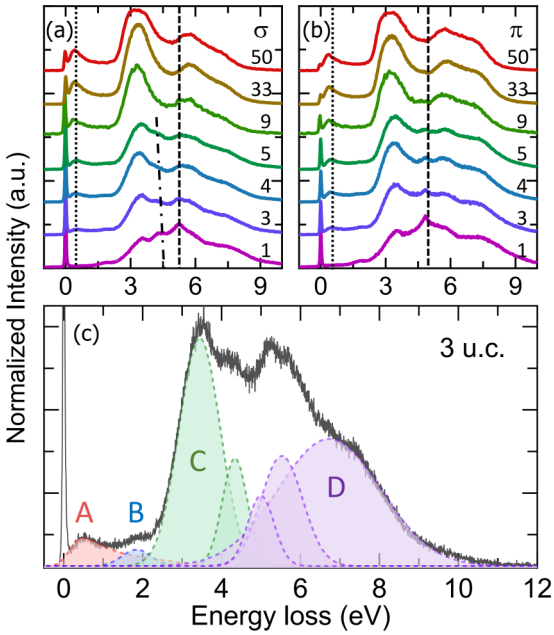

FIG. 3. (a) and (b) RIXS spectra at the O K edge with σ and π polarizations for $SrRuO_3$ thin films. (a) and (b) show the overall features of RIXS spectra depending on the thickness of the samples and the polarization of the incident beam. As the thickness decreases, the peak on the low-energy side (dot line) becomes weaker, while the peak at 5 eV (dashed line) gets stronger for both polarizations. In addition to the 5 eV peak, the peak around 4.5 eV (dash-dotted line) also appears for the σ polarization. Note that this 4.5 eV peak becomes stronger below the 5-u.c. sample and shifts towards higher energy with decreasing thickness. (c) The whole spectrum for the 1-u.c. sample with σ polarization. Altogether, seven Gaussian fitting functions are needed to fit the spectra based on the CI and DFT calculations. Different types of peaks are marked by different letters in (c).

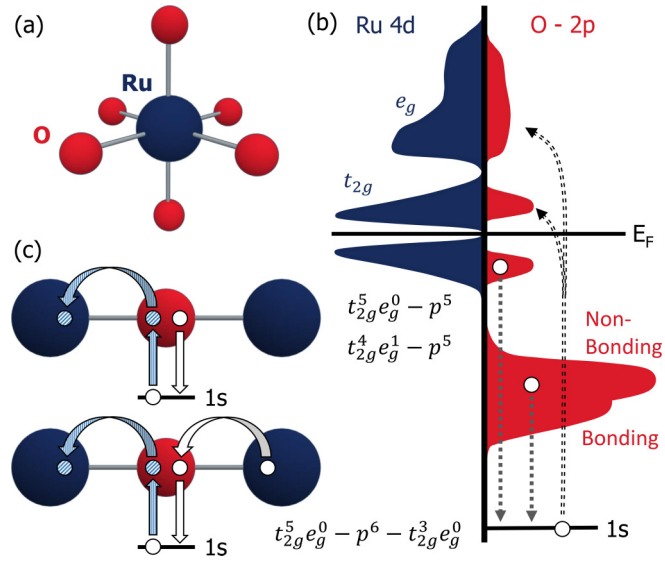

FIG. 4. (a) RuO_6 cluster used in the CI calculation. (b) and (c) Schematic view of charge transfer and d-d excitations. Oxygen 1s electrons are excited to vacant 2p levels which are hybridized with Ru t_{2g} orbitals. The energy losses should be different depending on orbitals from which the relaxation occurs. The top panel in (c) shows t_{2g}-e_g excitations, and the bottom one indicates the charge transfer from O 2p to Ru 4d levels.

energy of the peaks and their apparent relevance to our two main questions: QCE and MIT. For example, on the high-energy side ranging from 2 to 10 eV there are several strong peaks, marked as C and D. These peaks are due to the charge transfer from O 2p to Ru 4d orbitals and so reflect the expected change in the Ru 4d orbitals. On the other hand, there are two relatively weaker peaks below 2 eV with a strong thickness dependence. These low-energy excitations can be interpreted as arising from d-d excitations or coherent peaks connected to quasiparticle states that are closely related to the metallic phase of $SrRuO_3$. In the remainder of this paper, we focus on the charge transfers to explain the QCE first and then move on to the low-energy part for the MIT.

III. RESULTS AND DISCUSSION

A. Configuration interaction calculation of cluster models

In order to explain the charge transfer peaks and d-d excitations in detail, we performed the configuration interaction (CI) calculations using two cluster models of RuO_6 and Ru-O-Ru [see Fig. 4(a)] and found that each of the calculations with different clusters shows distinct features of $SrRuO_3$. We note that our model calculation suits t_{2g} orbitals of a more localized character. For instance, this calculation with the RuO_6 cluster model has the advantage of explaining the charge transfer between O 2p and Ru d orbitals because the cluster consists of six oxygen atoms. On the other hand, the calculation with the Ru-O-Ru cluster gives a better description of intersite d-d excitations. These calculations can also reflect the QCE by the extra control of adjusting the amount of Ru d splitting. For example, we can set Ru d orbitals to split into $\varepsilon_{xy} = 2/3\Delta_{t_{2g}}$, $\varepsilon_{xz} = \varepsilon_{yz} = -1/3\Delta_{t_{2g}}$, $\varepsilon_{z^2} = 10Dq - 1/2\Delta_{e_g}$, and $\varepsilon_{x^2-y^2} = 10Dq + 1/2\Delta_{e_g}$. It should be noted that we used an unusually large energy splitting between d_{xy} and d_{xz} (d_{yz}) orbitals ($\Delta_{t_{2g}} = 0.8$ eV) from the results of the first-principles calculation in Ref. [20], which is the energy difference between the 2D-type singularity of d_{xy} and the 1D-type singularity of d_{xz} (d_{yz}).

We also take into account both the spin-orbit coupling λ and the Kanamori-type Coulomb interaction (U and J_H) among d orbitals [27]. The energy levels of oxygen p orbitals in the valence band can depend on whether they are hybridized with Ru d orbitals or not [28–30]. For example, O p orbitals are assumed in our calculations to be noninteracting, and their energy levels are given as e_p for nonbonding p orbitals and $e_p - \Delta_p$ for bonding p orbitals. Here, e_p is determined as $e_p = 4U - 7J_H - \Delta$, where Δ is the charge transfer energy in the cubic symmetry defined as the energy difference between the lowest $d^5\underline{L}$ and d^4 states. The hopping integrals between p and d orbitals are parameterized by $V_{pd\pi}$ for t_{2g} orbitals and $V_{pd\sigma}$ for e_g orbitals according to the Slater-Koster theory [31]. We used the parameters shown in Table I in order to fit the experimental RIXS spectrum.

For more details on our calculations, let $|\Psi_g\rangle$ and E_g be the ground state and its energy, respectively. In the dipole and fast collision approximation, the oxygen K-edge RIXS intensity

TABLE I. Physical parameters used for the cluster calculations (in eV).

$10Dq$	$\Delta_{t_{2g}}$	Δ_{e_g}	λ	U	J_H	Δ	Δ_p	$V_{pd\sigma}$	$V_{pd\pi}$
2.1	0.8	0.4	0.1	2.0	0.3	3.3	1.6	−1.0	0.46

at zero momentum is given as

$$I \sim -\frac{1}{\pi}\mathrm{Im}\langle\Psi_g|\hat{R}(\boldsymbol{\epsilon},\boldsymbol{\epsilon}')\frac{1}{\omega - H + E_g + i\delta}\hat{R}(\boldsymbol{\epsilon},\boldsymbol{\epsilon}')|\Psi_g\rangle. \tag{1}$$

And $\hat{R}(\boldsymbol{\epsilon},\boldsymbol{\epsilon}')$ is the RIXS scattering operator, given as

$$\hat{R}(\boldsymbol{\epsilon},\boldsymbol{\epsilon}') = \frac{1}{3}\sum_{imm'\sigma}\epsilon_m\epsilon'_{m'}c_{im'\sigma}c^{\dagger}_{im'\sigma}, \tag{2}$$

where $c^{\dagger}_{im'\sigma}$ is the creation operator of the oxygen p electron with the $m = (x, y, z)$ orbital and σ spin at the ith site and $\boldsymbol{\epsilon}$ and $\boldsymbol{\epsilon}'$ are the polarizations of incident and outgoing x rays, respectively [27]. Here, δ is the Lorentz broadening, and we set $\delta = 0.2$ eV for our calculations.

In our calculations, p-orbital states can be expressed with a linear combination of bonding and nonbonding states as

$$c^{\dagger}_{im\sigma} = \sum_{\alpha}\left(U^{B}_{\alpha,im}\right)^{*}c^{\dagger}_{\alpha\sigma} + \sum_{\mu}\left(U^{N}_{\mu,im}\right)^{*}c^{\dagger}_{\mu\sigma}, \tag{3}$$

where $U^{B}_{\alpha,im}$ and $U^{N}_{\mu,im}$ are the coefficients of the m orbital at the ith site for bonding and nonbonding states α and μ, respectively. Because nonbonding p orbitals are fully occupied in the ground state, only the annihilation operation is allowed. We can then get the scattering operator associated with nonbonding orbitals as follows:

$$\hat{R}^{N}(\boldsymbol{\epsilon},\boldsymbol{\epsilon}') = \sum_{\alpha\mu\sigma}R^{N}_{\alpha\mu}(\boldsymbol{\epsilon},\boldsymbol{\epsilon}')c_{\mu\sigma}c^{\dagger}_{\alpha\sigma}, \tag{4}$$

where $R^{N}_{\alpha\mu} = \frac{1}{3}\sum_{imm'}U^{N}_{\mu,im'}(U^{B}_{\alpha,im})^{*}\epsilon'_{m'}\epsilon_m$. The RIXS intensity attributed to nonbonding p orbitals is given as

$$I^{N} = -\frac{1}{\pi}\mathrm{Im}\sum_{\alpha\alpha'\mu}R^{N}_{\alpha'\mu}(\boldsymbol{\epsilon},\boldsymbol{\epsilon}')^{*}R^{N}_{\alpha\mu}(\boldsymbol{\epsilon},\boldsymbol{\epsilon}') \times\langle\Psi_g|c_{\alpha'\sigma}\frac{1}{\omega - H + E_g + e_p + i\delta}c^{\dagger}_{\alpha'\sigma}|\Psi_g\rangle. \tag{5}$$

The RIXS intensity attributed to the bonding p orbitals can then be calculated using the following relation:

$$I^{B} = -\frac{1}{\pi}\mathrm{Im}\langle\Psi_g|\hat{R}^{B}(\boldsymbol{\epsilon},\boldsymbol{\epsilon}')\frac{1}{\omega - H + E_g + i\delta}\hat{R}^{B}(\boldsymbol{\epsilon},\boldsymbol{\epsilon}')|\Psi_g\rangle, \tag{6}$$

where

$$\hat{R}^{B}(\boldsymbol{\epsilon},\boldsymbol{\epsilon}') = \frac{1}{3}\sum_{\alpha\beta\sigma imm'}U^{B}_{\beta,im'}\left(U^{B}_{\alpha,im}\right)^{*}\epsilon'_{m'}\epsilon_m c_{\beta\sigma}c^{\dagger}_{\alpha\sigma}. \tag{7}$$

In the case of the CI calculation of a Ru-O-Ru cluster, mainly explaining the low-energy excitations, we directly used Eqs. (1) and (2) instead of considering bonding and nonbonding states. In addition, we restricted the Hilbert space with the assumption that the oxygen atom between two Ru atoms has three possible states, p^4, p^5, and p^6 electron configurations. The result of this calculation is shown in Fig. 5.

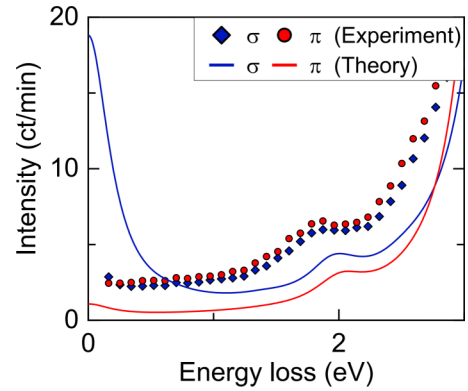

FIG. 5. Low-energy RIXS spectra of 1-u.c. $SrRuO_3$ with the CI calculation of a Ru-O-Ru cluster. The symbols represent the experimental results, while the lines show the theoretical results, with different colors used for the different polarizations of the incident beam. The peak at 2 eV shows intersite d-d excitations.

The peaks in the O K-edge RIXS spectrum can also be categorized according to Ru $4d$ orbitals that participate in the RIXS process, as shown in Fig. 4. Electrons in the core oxygen levels are excited to vacant O $2p$ levels that are hybridized with Ru $4d$ orbitals as seen in the O K-edge RIXS, and the subsequent relaxation occurs from the occupied $2p$ states. We can, in principle, determine the origin of each peak by examining the energy of the emitted photons. For example, if the electrons are relaxed from the $2p$ level hybridized with t_{2g} levels that are located right below the Fermi level, the process can be considered d-d excitations. In the case of charge transfers between the $2p$ and $4d$ orbitals, however, the relaxation starts from the $2p$ states not participating in the hybridization.

B. Quantum confinement effects

According to our CI calculations, the charge transfers correspond to peaks C and D as observed from 2 to 10 eV. Peak C, for instance, represents the charge transfer between nonbonding O $2p$ states and Ru t_{2g} orbitals, while peak D mainly originates from bonding O $2p$ states and Ru e_g orbitals. As shown in the top graphs of Fig. 3, both peaks C and D undergo a considerable change depending on the thickness of the sample and the polarization of the incident beam. The remarkable change in peak C is clearly seen around 4.4 eV. It is notable that this variation occurs only for the σ polarization. Meanwhile, an additional peak emerges around 5 eV that is most likely due to the charge transfer between O $2p$ and Ru e_g levels in both polarization channels, but the position of the peak is slightly different depending on the polarization (see Fig. 6).

The splitting of both peaks shown in Figs. 3 and 6 can be taken as evidence of the QCE, which is more pronounced for the thinner samples. The splitting of peaks around 4 and 5 eV reflects the energy splitting of Ru t_{2g} and e_g, respectively. Of interest, the QCE in monolayer $SrRuO_3$ modifies the

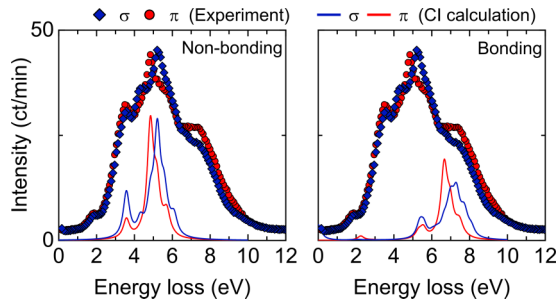

FIG. 6. RIXS spectra with the results of CI calculation for monolayer $SrRuO_3$. The symbols represent the experimental results, while the lines show the theoretical results, with different colors used for the different polarizations of the incident beam. (Left) Calculation results with nonbonding p orbitals; (right) calculation results with bonding states.

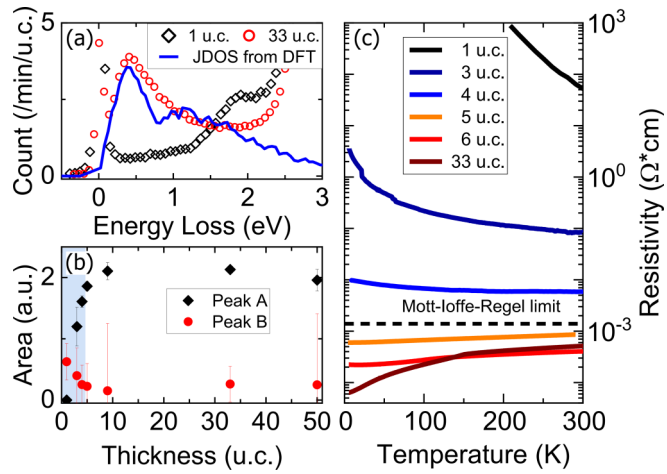

FIG. 7. (a) and (b) Low-energy excitations are compared to the JDOS from the DFT calculation. We clearly observe the electron-hole continuum in the thick sample, which arises from its metallic phase. The intensity of peak A sharply decreases below 5 u.c., and it completely disappears for the monolayer $SrRuO_3$. (c) Electrical resistivity of $SrRuO_3$ thin films with different thickness. The resistivity increases progressively with reducing the thickness and crosses the theoretical Mott-Ioffe-Regel limit between 4 and 5 u.c. It is notable that the critical thickness from RIXS and the resistivity coincide with one another.

electronic structure, which subsequently induces the separate orbital energy levels depending on the geometrical characteristics of each orbital. We comment that the energy difference between each singularity of the 2D-type band for d_{xy} and the 1D-type band of d_{xz} (d_{yz}) corresponds quite well to the amount of peak splitting in peak C [20]. It should also be noted that 0.8 eV of t_{2g} energy splitting cannot be obtained in the cases of the usual Jahn-Teller distortion, which is typically about 0.1 eV for t_{2g} of ruthenates [32].

A further interesting point is the polarization dependence of the peaks. In our explanation, the QCE pushes the energy levels of d_{xz} (d_{yz}) or d_{z^2} down, so that the energy of charge transfer related to those orbitals gets shifted towards lower energy. On the other hand, orbitals such as d_{xy} and $d_{x^2-y^2}$ move in the opposite direction. In the case of the charge transfer between d_{xz} (d_{yz}) and p orbitals, the same amount of energy shift compensates for the hopping integral $V_{pd\pi}$. Thus, the additional peak at 4.4 eV appears only with the orbitals parallel to the surface of the samples, and the one around 5 eV emerges at different energies depending on the polarization of the incident beam. Because each polarization excites different O p orbitals, we believe the "orbital-selective" characteristic of the QCE results in the observed polarization dependence.

C. Metal-insulator transition

While the peaks related to the charge transfer seem to support our scenario of the QCE process in $SrRuO_3$ films, the ones in the low-energy range produce the clearest evidence of MIT. For instance, with decreasing thickness peak A is suppressed rapidly, but peak B gets enhanced simultaneously below the thickness of 5 u.c. The opposite trends of peaks A and B can be easily understood in terms of MIT, as seen in the resistivity data shown in Fig. 7. We note that the critical thickness can depend on the growth conditions, according to our fabrication of several $SrRuO_3$ films used for this work.

According to our CI calculations, peak B can be ascribed to d-d excitations between intersite t_{2g} orbitals [Fig. 4(c)]. Electrons are excited to O $2p$ levels that hybridize with Ru t_{2g} levels in the valence band, and afterwards, relaxation occurs from the t_{2g} levels in the conduction band. Although the process can, in principle, involve oxygen p levels, it is intrinsically the excitations between two separate t_{2g} bands in the valence and conduction bands.

Meanwhile, the origin of peak A can be found by calculating the joint density of states (JDOS) from first-principles calculations with density functional theory. The JDOS represents the probability of allowed interband transitions including absorption or energy-loss functions [33,34]. We calculated the JDOS by considering the energy levels in the valence and conduction bands. In our calculation, the JDOS is given as

$$J(\boldsymbol{q}) = \sum_{\vec{k}} \delta[|\varepsilon_f(\boldsymbol{k}) - \varepsilon_i(\boldsymbol{k}-\boldsymbol{q})|]. \tag{8}$$

According to our experimental geometry with a grazing angle, we choose an interband transition with fixed momentum transfer of $\mathbf{q}_\parallel = 0.28[2\pi/a]$ and compute the DOS of the energy difference between two levels, which represent the theoretical spectrum of electron-hole excitations. By comparing our calculation results with the experimental data, as shown in Fig. 7, the calculated JDOS for the electron-hole continuum is in good agreement with the lowest peak seen in bulk $SrRuO_3$. This means that peak A corresponds to itinerant quasiparticle excitations, while peak B corresponds to excitations between lower and upper Hubbard bands. In this sense, the spectral weight transfer from peak A to peak B is in good agreement with the MIT in $SrRuO_3$ thin films. We note that the transfer of spectral weight from peak A to peak B is also consistent with MIT, as seen in the resistivity data.

Another interesting point is the connection between the QCE and MIT, whose experimental evidence can be readily found in the very thin $SrRuO_3$ sample. In particular, a new peak is seen to be separated from the d_{xy} level below 5 u.c. and moves towards higher energy, as shown in Fig. 6. This means

that the QCE gets enhanced in thinner $SrRuO_3$ samples. With the QCE splitting the Ru 4*d* bands, the MIT in $SrRuO_3$ resembles that of Ca_2RuO_4, which is a classic example of an orbital-selective Mott insulator [35]. For our thinnest sample of 1 u.c. $SrRuO_3$, the QCE seems to split the otherwise degenerate t_{2g} orbitals, leading to a Mott-type insulating state. Therefore, we can maintain that a new way of realizing a Mott-type insulating phase is found in the ultrathin $SrRuO_3$ sample with thickness being a control parameter, which is different from the bulk sample.

IV. CONCLUSION

To conclude, the good agreement between the theoretical calculation and the experimental observation of charge-transfer peak splitting in the RIXS spectra suggests the orbital-selective QCE in ultrathin $SrRuO_3$ films. We also found that the suppression of the low-energy excitations arises from the electron-hole continuum across the metal-insulator transition. Finally, our studies provide clear experimental evidence that the QCE leads to a Mott insulating phase in ultrathin $SrRuO_3$.

ACKNOWLEDGMENTS

We would like to acknowledge D. Khomskii and B. Kim for helpful discussions. The work at IBS CCES is supported by the Institute of Basic Science (IBS) in Korea (Grants No. IBS-R009-G1, No. IBS-R009-G2, and No. IBS-R009-D1). The work at the Paul Scherrer Institut is supported by the Swiss National Science Foundation through NCCR MARVEL and the Sinergia network Mott Physics Beyond the Heisenberg Model (MPBH). We also thank the Korea Institute for Advanced Study for providing computing resources (KIAS Center for Advanced Computation Linux Cluster System) for this work.

[1] K. I. Kugel and D. I. Khomski, Sov. Phys. Usp. **25**, 231 (1982).
[2] M. B. Salamon and M. Jaime, Rev. Mod. Phys. **73**, 583 (2001).
[3] S. Lee, J.-G. Park, D. T. Adroja, D. Khomskii, S. Streltsov, K. A. McEwen, H. Sakai, K. Yoshimura, V. I. Anisimov, D. Mori, R. Kanno, and R. Ibberson, Nat. Mater. **5**, 471 (2006).
[4] L. Das, F. Forte, R. Fittipaldi, C. G. Fatuzzo, V. Granata, O. Ivashko, M. Horio, F. Schindler, M. Dantz, Y. Tseng, D. E. McNally, H. M. Rønnow, W. Wan, N. B. Christensen, J. Pelliciari, P. Olalde-Velasco, N. Kikugawa, T. Neupert, A. Vecchione, T. Schmitt, M. Cuoco, and J. Chang, Phys. Rev. X **8**, 011048 (2018).
[5] J. S. Lee, S. J. Moon, T. W. Noh, S. Nakatsuji, and Y. Maeno, Phys. Rev. Lett. **96**, 057401 (2006).
[6] M. S. Laad, L. Craco, and E. Muller-Hartmann, Phys. Rev. B **73**, 045109 (2006).
[7] S. Kim, K. Kim, C.-J. Kang, and B. I. Min, Phys. Rev. B **87**, 195106 (2013).
[8] S. V. Streltsov and D. I. Khomskii, Proc. Natl. Acad. Sci. USA **113**, 10491 (2016).
[9] S. Y. Jang, H. Kim, S. J. Moon, W. S. Choi, B. C. Jeon, J. Yu, and T. W. Noh, J. Phys.: Condens. Matter **22**, 485602 (2010).
[10] M. Neupane, P. Richard, Z.-H. Pan, Y.-M. Xu, R. Jin, D. Mandrus, X. Dai, Z. Fang, Z. Wang, and H. Ding, Phys. Rev. Lett. **103**, 097001 (2009).
[11] H. N. Lee, H. M. Christen, M. F. Chisholm, C. M. Rouleau, and D. H. Lowndes, Appl. Phys. Lett. **84**, 4107 (2004).
[12] L. Klein, J. S. Dodge, C. H. Ahn, J. W. Reiner, L. Mieville, T. H. Geballe, M. R. Beasley, and A. Kapitulnik, J. Phys.: Condens. Matter **8**, 10111 (1996).
[13] K. D. Sung, Y. A. Park, N. Hur, and J. H. Jung, J. Korean Phys. Soc. **52**, 1955 (2008).
[14] A. T. Zayak, X. Huang, J. B. Neaton, and K. M. Rabe, Phys. Rev. B **74**, 094104 (2006).
[15] S. Lee, J. R. Zhang, S. Torii, S. Choi, D.-Y. Cho, T. Kamiyama, J. Yu, K. A. McEwen, and J.-G. Park, J. Phys.: Condens. Matter **25**, 465601 (2013).
[16] S. Itoh, Y. Endoh, T. Yokoo, S. Ibuka, J.-G. Park, Y. Kaneko, K. S. Takahashi, Y. Tokura, and N. Nagaosa, Nat. Commun. **7**, 11788 (2016).
[17] A. P. Mackenzie, J. W. Reiner, A. W. Tyler, L. M. Galvin, S. R. Julian, M. R. Beasley, T. H. Geballe, and A. Kapitulnik, Phys. Rev. B **58**, R13318(R) (1998).
[18] D. Toyota, I. Ohkubo, H. Kumigashira, M. Oshima, T. Ohnishi, M. Lippmaa, M. Takizawa, A. Fujimori, K. Ono, M. Kawasaki, and H. Koinuma, Appl. Phys. Lett. **87**, 162508 (2005).
[19] J. Xia, W. Siemons, G. Koster, M. R. Beasley, and A. Kapitulnik, Phys. Rev. B **79**, 140407 (2009).
[20] Y. J. Chang, C. H. Kim, S.-H. Phark, Y. S. Kim, J. Yu, and T. W. Noh, Phys. Rev. Lett. **103**, 057201 (2009).
[21] R. M. Martin, *Electronic Structure: Basic Theory and Practical Methods* (Cambridge University Press, Cambridge, 2004).
[22] J. Liu, S. Okamoto, M. van Veenendaal, M. Kareev, B. Gray, P. Ryan, J. W. Freeland, and J. Chakhalian, Phy. Rev. B **83**, 161102 (2011).
[23] V. N. Strocov, T. Schmitt, U. Flechsig, T. Schmidt, A. Imhof, Q. Chen, J. Raabe, R. Betemps, D. Zimoch, J. Krempasky, X. Wang, M. Grioni, A. Piazzalunga, and L. Patthey, J. Synchrotron Radiat. **17**, 631 (2010).
[24] G. Ghiringhelli, A. Piazzalunga, C. Dallera, G. Trezzi, L. Braicovich, T. Schmitt, V. N. Strocov, R. Betemps, L. Patthey, X. Wang, and M. Grioni, Rev. Sci. Instrum. **77**, 113108 (2006).
[25] J. Park, B.-G. Cho, K. D. Kim, J. Koo, H. Jang, K.-T. Ko, J.-H. Park, K.-B. Lee, J.-Y. Kim, D. R. Lee, C. A. Burns, S. S. A. Seo, and H. N. Lee, Phys. Rev. Lett. **110**, 017401 (2013).
[26] M. Salluzzo, G. Ghiringhelli, N. B. Brookes, G. M. De Luca, F. Fracassi, and R. Vaglio, Phys. Rev. B **75**, 054519 (2007).
[27] B. H. Kim and J. van den Brink, Phys. Rev. B **92**, 081105(R) (2015).
[28] J. Park, S.-J. Oh, J.-H. Park, D. M. Kim, and C.-B. Eom, Phys. Rev. B **69**, 085108 (2004).
[29] J. Kim, J. Chung, and S.-J. Oh, Phys. Rev. B **71**, 121406 (2005).
[30] K. Maiti and R. S. Singh, Phys. Rev. B **71**, 161102 (2005).

[31] J. C. Slater and G. F. Koster, Phys. Rev. **94**, 1498 (1954).
[32] G. Cao and L. DeLong, *Frontiers of 4d- and 5d-Transition Metal Oxides* (World Scientific, Singapore, 2013).
[33] W. Y. Liang and A. R. Beal, J. Phys. C **9**, 2823 (1976).
[34] C. I. Cabrera, D. A. Contreras-Solorio, and L. Hernández, Phys. E (Amsterdam, Neth.) **76**, 103 (2016).
[35] D. Sutter, C. G. Fatuzzo, S. Moser, M. Kim, R. Fittipaldi, A. Vecchione, V. Granata, Y. Sassa, F. Cossalter, G. Gatti, M. Grioni, H. M. Rønnow, N. C. Plumb, C. E. Matt, M. Shi, M. Hoesch, T. K. Kim, T.-R. Chang, H.-T. Jeng, C. Jozwiak, A. Bostwick, E. Rotenberg, A. Georges, T. Neupert, and J. Chang, Nat. Commun. **8**, 15176 (2017).